Study of the Damping Capacity of Structural Joints Made of Graphite Epoxy Composite Material

Mohan D. Rao

Department of Mechanical Engineering-Engineering Mechanics
Michigan Technological University
Houghton, MI 49931

and

Malcolm J. Crocker, and P.K. Raju
Department of Mechanical Engineering
Auburn University
Auburn, AL 36849

ABSTRACT

Owing to their high strength and low weight, composite materials have found applications in commercial, military, and spacecraft structures. The truss system of the Hubble Space Telescope, for example, is made of graphite epoxy beams, tubes and joints that have very low damping capacity. Vibration of the Space Telescope is undesirable since it would cause blurring of the optical system images. A specific knowledge of the damping capacity of the composite material and structural joints and the factors that influence the damping is very useful in the design of appropriate vibration isolation systems for the telescope.

Joints form an important aspect of any space structural system. Unlike metals, fiber composites cannot be welded together. The alternatives include the use of mechanical fasteners, such as bolts and rivets or adhesive bonding. These techniques produce joints with vastly different properties. it is believed that bonded (and bolted) joints act to enhance the damping capacity of structural systems. Hence in this paper the results of analytical and experimental investigations carried out on two different types of joint composite specimens to study their damping capacity are reported.

First, a theoretical model to study the Vibration of a bonded lap joint system was developed and is described. The model can be used to predict the natural frequencies, modal damping ratios and mode shapes of the system for free flexural vibration. Good agreement between numerical and experimental results was obtained for a system of graphite epoxy beams lap-jointed by an epoxy adhesive.

The second type of bonded joint considered for the study was a double-butt joint. Experimental work conducted on these joints in a vacuum chamber is described. The damping ratio was computed by using an improved half-power points method. The increase in the values of the damping ratio due to the presence of bonded joints in the system does not appear to be very significant.

INTRODUCTION

Structural adhesive bonding of composites to composites, as well as composites to metallic components, has developed rapidly due to advances in composite materials and adhesive bonding techniques. Structural composite bonded joints are primarily of the overlap type (single or double overlap). Scarf joints are structurally efficient, but are difficult or costly to manufacture. Butt joints, although simple to process, are not considered for primary structural joints. This is because of their limited load carrying capacity due to the presence of cleavage stresses when the loading is not a true tensile load. Tube joints are difficulty and costly to manufacture.

The paper by Goland and Reissner [1] is regarded as a classic work in the area of static analysis of a simple lap joint. Goland and Reissner studied the stresses in bonded single lap joints for two different cases. In the first case, the bond layer was very thin, in the second case, the bond layer was so thick that it was the primary contributor to joint flexibility. In both cases, they derived equations to evaluate the shearing and normal stresses in the bond layer as well as those in the jointed plates. In the Goland and Reissner analysis, the peel and shear stresses were assumed to be constants across the adhesive thickness. In later works by Ojalvo and Eidinoff [2], Carpentor [3], and Kline [4], attempts are made to incorporate a linear variation of these stresses across the thickness of the adhesive. Delale and Erdogan [5] have carried out the stress analysis of a bonded lap joint system assuming that the adherents are elastic and the adhesive is linearly viscoelastic. Renton and Vinson [6], and Delale, Erdogan, and Aydinoglu [7] have attempted to include anisotropic adherents in the mathematical model.

Hart-Smith [8-11] was the first investigator to extensively use continuum mechanics approach in the analysis of bonded joints. He has analyzed double-lap, single-lap, scarf, stepped-lap and tapered-lap configurations. Tensile, compressive and in-plane shear stresses in the system were considered based on an elastic-plastic analysis of the configuration. In that work, the author has also discussed joint efficiency and potential failure modes for each of the above configurations. The above review indicates that much of the work done in this area has been confined to the static analysis of bonded joints.

I. ANALYTICAL MODELING OF FLEXURAL VIBRATION OF A BONDED LAP-JOINT SYSTEM

The system chosen for study is shown in Figure 1. The objective is to arrive at a suitable mathematical model to evaluate the damping ratios and resonance frequencies of the system undergoing free flexural vibration. The system consists of a pair of rectangular beams lap-jointed over a certain length. The bond between the two beams is achieved by means of an adhesive whose thickness is small compared with those of the beams. The unjointed ends of the beams may have any physically realizable boundary conditions, but, in this case are assumed to be simply-supported. Equations of motion are first derived using the complex modulus approach, assuming the beams to be made of composite materials. The adhesive is assumed to be linearly viscoelastic and the widely used Kelvin-Voight model is used to represent the viscoelastic behavior of the adhesive.

The starting point for the development of this model is the consideration of the dynamic equilibrium equations of the overlap (joint) region. The equations of motion in the joint region are derived using a differential element approach. The transverse displacements of the upper and the lower beam are considered to be different. The normal force between each beam and

the adhesive layer is obtained from the Kelvin-Voight viscoelastic model of the adhesive. The shear force at the interface between the adhesive and the beam is obtained from the simple bending motion equations of the two beams. The resulting equations of motion are combined with the equations of transverse vibration of the beams in the unjointed regions. These are later solved as a boundary value problem by knowledge of the boundary conditions at the unjointed ends and the motion continuity equations at the ends of the overlap. The eigenvalues and the eigenvectors of the system are obtained numerically by an iterative technique on a computer.

The beam system is hypothetically divided into three parts as shown in Figure 2. The coordinate system chosen for each part is also shown in the same figure.

Analysis of Part 1 of Beam System

The following assumptions are made in the analysis: a) the analysis is carried out only for the free flexural vibration of the system; the longitudinal and rotary inertia effects are neglected, b) there is no slip at the bond interfaces, c) all points on a plane normal to the longitudinal axis of the beam have the same transverse displacement, d) the longitudinal force in the adhesive layer may be neglected relative to those in the beams, and e) since the thickness of the adhesive layer is small relative to the thickness of the beam, the mass (inertia) of the adhesive may be neglected, and the normal and shear forces in the adhesive are assumed to be constant.

A free-body diagram of a differential element of length dx of the composite three-layer part of the beam system is shown in Figure 3. N is the axial force in the beam, V represents the shear force in the beams, M is the bending moment in the beam, s is the shear force per unit length at the bond interfaces, and p is the transverse force per unit length between the beam and the adhesive. The above quantities with subscript 1 refer to the upper beam and with subscript 2 refer to the lower beam. Furthermore, $y_1 = y_1(x,t)$ is the transverse displacement of the upper beam, and $y_2 = y_2(x,t)$ is that of the lower beam.

Equating the sum of the forces in the y-direction to the corresponding inertia forces, we get for beam 1,

$$-V_1 + \left[V_1 + \frac{\partial V_1}{\partial x}\,dx\right] + p\,dx = \rho_1 A_1\,dx\,\frac{\partial^2 y_1}{\partial t^2}\,, \qquad (1)$$

and for beam 2

$$-V_2 + \left[V_2 + \frac{\partial V_2}{\partial x}\,dx\right] + p\,dx = \rho_2 A_2\,dx\,\frac{\partial^2 y_2}{\partial t^2}\,. \qquad (2)$$

The term ρA in Equations (1) and (2) is the mass per unit length, in which ρ represents the density and A represents the cross sectional area of the beam. Summing the moments about the center of the right edge, for beam 1,

$$M_1 - \left(M_1 + \frac{\partial M_1}{\partial x}\,dx\right) - s\,dx\,\frac{h_1}{2} + V_1\,dx = 0\,. \qquad (3)$$

for beam 2,

$$M_2 - \left(M_2 + \frac{\partial M_2}{\partial x}\,dx\right) - s\,dx\,\frac{h_2}{2} + V_2\,dx = 0\,. \qquad (4)$$

From Equation (1) through (4), we have,

$$\frac{\partial^2 M_1}{\partial x^2} + \frac{h_1}{2}\frac{\partial s}{\partial x} + p = \rho_1 A_1 \frac{\partial^2 y_1}{\partial t^2}, \text{ and} \tag{5}$$

$$\frac{\partial^2 M_2}{\partial x^2} + \frac{h_2}{2}\frac{\partial s}{\partial x} - p = \rho_2 A_2 \frac{\partial^2 y_2}{\partial t^2}. \tag{6}$$

Equations (5) and (6) represent the equations of motion for the upper and lower beam respectively. From the classical theory of pure bending of beams, the bending moments M_1 and M_2 may be related to the corresponding transverse displacements, y_1 and y_2 through the flexural rigidity term EI, where E is the Young's modulus of the material of the beam, and I is the second moment of the cross-sectional area with respect to the centroidal axis. Noting that the y-axis is positive downwards, from beam theory,

$$M_1 = - E_1 I_1 \frac{\partial^2 y_1}{\partial x^2} \text{ and } M_2 = - E_2 I_2 \frac{\partial^2 y_2}{\partial x^2}. \tag{7}$$

It should be noted that Equation (7) is valid for an elastic, homogeneous beam having a constant cross-sectional area. It turns out, however, that an equation similar to the above can be written for the composite beams of the present problem, by simply replacing the real modulus by its complex counterpart. This analysis is valid only for simple harmonic time dependence. With this in mind, we can write,

$$M_1 = - E_1^* I_1 \frac{d^2 y_1}{dx^2} \text{ and } M_2 = - E_2^* I_2 \frac{d^2 y_2}{dx^2}. \tag{8}$$

where $E_1^* = E_1(1 + i\alpha\omega)$, and $E_2^* E_2(1 + i\beta\omega)$. (9)

α and β are some constants whose values depend on the material, ω is the angular frequency, and $i = \sqrt{-1}$. The next objective is to find suitable expressions for p and s in terms of y_1 and y_2, so that Equations (5) and (6) can be solved.

As mentioned before, the adhesive layer is modeled as a Kelvin-Voight viscoelastic solid, because of the mathematical simplicity. A detailed derivation of a standard-linear model for a viscoelastic material and its reduction to a Kelvin-Voight model can be found in Reference [12]. Accordingly, we can write,

$$p = K (y_1 - y_2) + c \left(\frac{\partial y_1}{\partial t} - \frac{\partial y_2}{\partial t}\right). \tag{10}$$

K refers to the transverse stiffness per unit length, and c is the viscous damping coefficient. K may be related to the storage modulus E_c, the width b, and the thickness h_c of the adhesive by, $K = E_c b/h_c$.

The interfacial shear force s may be found by considering a small element of the viscoelastic layer as shown in Figure 4. The element is deformed due

to the axial displacements, u_1 and u_2 of the bonded surfaces of beams 1 and 2 respectively, caused by their bending moments. For small displacements, the shear stress τ, is related to shear strain in the adhesive by:

$$\tau = G_c \left\{\frac{u_1 - u_2}{h_c}\right\} + \gamma \frac{\partial}{\partial t} \left\{\frac{u_1 - u_2}{h_c}\right\} . \tag{11}$$

The expression on the right hand side excluding G_c is the shear strain. G_c is the real part of the shear modulus of the adhesive material. As before, γ is another constant which is included here to take care of the viscoelastic nature of the adhesive.

Assume that the axial deformations, u_1 and u_2 are caused only by the bending of the beams and that there are no external axial forces in the beams. Then, from the classical theory of pure bending of beams, it can be shown that

$$u_1 = \frac{h_1}{2} \frac{\partial y_1}{\partial x} , \text{ and } u_2 = - \frac{h_2}{2} \frac{\partial y_2}{\partial x} . \tag{12}$$

In deriving the above expressions, it is also assumed that the neutral axis of the upper beam always remains above that of the lower beam. Then,

$$u_1 - u_2 = \frac{h_1}{2} \frac{\partial y_1}{\partial x} + \frac{h_2}{2} \frac{\partial y_2}{\partial x} . \tag{13}$$

From Equations (11) and (13), the interfacial shear force per unit length s is given by

$$s = \frac{G_c b}{2h_c} \left[(h_1 \frac{\partial y_1}{\partial x} + h_2 \frac{\partial y_2}{\partial x}) + \gamma \frac{\partial}{\partial t} (h_1 \frac{\partial y_1}{\partial x} + h_2 \frac{\partial y_2}{\partial x})\right]. \tag{14}$$

It is interesting to note here that for a simple harmonic time dependence of the form, $e^{i\omega t}$ for y_1 and y_2, Equations (10) and (14) can be written in a more familiar form as

$$p = K_c^* [y_1 - y_2], \tag{15}$$

and

$$s = \frac{G_c^* b}{2h_c} [h_1 \frac{dy_1}{dx} + h_2 \frac{dy_2}{dx}], \tag{16}$$

where

$$K_c^* = K(1 + i \frac{c\omega}{K}), \text{ and } G_c^* = G_c (1 + i\gamma\omega). \tag{17}$$

K_c^* and G_c^* may be considered as the complex stiffness and complex shear modulus of the adhesive material respectively.

The next step is to obtain the final form of the equations of the motion (5) and (6) by making use of the relations developed so far for M_1, M_2, p and s. This is easily done by noting that $y_1 = Y_1 e^{i\omega t}$, and $y_2 = Y_2 e^{i\omega t}$, where Y_1 and Y_2 are now functions of x only. ω is the complex natural frequency, the real part ω_R represents the damped natural frequency and the ratio of the imaginary part ω_I to ω_R represents the modal loss factor η. The modal damping ratio ζ is simply equal to $\eta/2$. Now, from Equations (5), (8), (15)

and (16), we obtain for the upper beam:

$$E_1 I_1 \frac{d^4 Y_1}{dx^4} - \frac{G_c^* b h_1}{4 h_c}\left[h_1 \frac{d^2 Y_1}{dx^2} + h_2 \frac{d^2 Y_2}{dx^2}\right] + K_c^* (Y_1 - Y_2) - \rho_1 A_1 \omega^2 Y_1 = 0, \quad (18)$$

and, similarly from Equations (6), (9), (15), and (16), we get for the lower beam:

$$E_2 I_2 \frac{d^4 Y_1}{dx^4} - \frac{G_c^* b h_2}{4 h_c}\left[h_1 \frac{d^2 Y_1}{dx^2} + h_2 \frac{d^2 Y_2}{dx^2}\right] - K_c^* (Y_1 - Y_2) - \rho_2 A_2 \omega^2 Y_2 = 0. \quad (19)$$

Here, $Y_1 = Y_1(x)$, $Y_2 = Y_2(x)$.

Equations (18) and (19) are coupled equations of motion of the system, the solution of which can be obtained by assuming a solution of the form $Y_1 = A_n e^{\lambda_n x}$, and $Y_2 = B_n e^{\lambda_n x}$.

Non-dimensionalization

The above equations of motion (18) and (19), should be expressed in a non-dimensional form so as to avoid overflow problems on the computer during the solution scheme. This is done in this section for the special case in which the two beams are assumed to be identical.

Let $E_1 = E_2 = E$, and $h_1 = h_2 = h$. The following non-dimensional parameters are used:

$$\bar{Y}_1 = \frac{Y_1}{h}, \quad \bar{Y}_2 = \frac{Y_2}{h}, \quad \bar{x} = \frac{X}{L}, \quad \bar{\ell} = \frac{\ell}{L},$$

where

$$L = \ell + \ell_c.$$

Also, let

$$\bar{G}_c = \frac{G_c}{E}, \quad \bar{E}_c = \frac{E_c}{E}, \quad \bar{h} = \frac{h}{L}, \quad \bar{\ell}_c = \frac{\ell_c}{L}.$$

The non-dimensional natural frequency is expressed as

$$\bar{\omega} = \frac{\omega}{\omega_o}, \text{ where } \omega_o^2 = \frac{EI}{\rho A L^4}. \quad (20)$$

Equations (4.24) and (4.25), written in non-dimensional form, are:

$$\frac{d^4 \bar{Y}_1}{d\bar{x}^4} - \frac{3\bar{G}_c^*}{\bar{h}\,\bar{h}_c}\left[\frac{d^2 \bar{Y}_1}{d\bar{x}^2} + \frac{d^2 \bar{Y}_2}{d\bar{x}^2}\right] + \frac{12\bar{E}_c}{\bar{h}_c \bar{h}^3}(\bar{Y}_1 - \bar{Y}_2) - \bar{\omega}^2 \bar{Y}_1 = 0, \quad (21)$$

and

$$\frac{d^4\bar{Y}_1}{d\bar{x}^4} - \frac{3\bar{G}_c^*}{\bar{h}\,\bar{h}_c}\left[\frac{d^2\bar{Y}_1}{d\bar{x}^2} + \frac{d^2\bar{Y}_2}{d\bar{x}^2}\right] + \frac{12\bar{E}_c}{\bar{h}_c\bar{h}^3}(\bar{Y}_1-\bar{Y}_2) - \bar{\omega}^2\,\bar{Y}_2 = 0. \qquad (22)$$

Here,

$$\bar{E}_c^* = \frac{E_c(1+i\eta_2)}{E(1+i\eta_1)}, \text{ and } \bar{G}_c^* = \frac{G_c(1+i\eta_2)}{E(1+i\eta_1)}. \qquad (23)$$

η_1 may be considered as the modal loss factors of the beam material, and η_2 and η_3 as the modal loss factors of the viscoelastic material in bending and shearing motions respectively. η_1, η_2 and η_3 may be assumed to have suitable values which depend on the material, when computing the eigenvalues and eigenvectors for each mode.

As mentioned before, Equations (21) and (22) can be decoupled by a series solution of the form

$$\bar{Y}_1 = A_n e^{\lambda_n \bar{x}}, \text{ and } \bar{Y}_2 = B_n e^{\lambda_n \bar{x}}, \qquad (24)$$

where A_n and B_n are constants to be determined from the boundary conditions. Substituting Equation (24) in (21) and (22), we obtain, a matrix of the form:

$$\begin{bmatrix} (\lambda_n^4 - C_1\lambda_n^2 + C_2 - \bar{\omega}^2) & -(C_1 + C_2) \\ -(C_1 + C_2) & (\lambda_n^2 - C_1\lambda_n^2 + C_2 - \bar{\omega}^2) \end{bmatrix} \begin{bmatrix} A_n \\ B_n \end{bmatrix} = 0 \qquad (25)$$

with

$$C_1 = \frac{3\,\bar{G}_c^*}{\bar{h}_c\,\bar{h}}, \quad C_2 = \frac{12\,\bar{E}_c^*}{\bar{h}_c\,\bar{h}^3}. \qquad (26)$$

For a non-trivial solution, the determinant of the above matrix set equal to zero yields eight roots of λ. Equation (25) yields eight unique roots for λ. Furthermore, from the above matrix, the constants A and B are related by:

$$B_n = \phi_n A_n,$$

where

$$\phi_n = \left[\frac{\lambda_n^4 - C_1\lambda_n^2 + C_2 - \bar{\omega}^2}{C_1 + C_2}\right]. \qquad (27)$$

Finally, we have

$$\bar{Y}_1 = \sum_{n=1}^{8} A_n e^{\lambda_n \bar{x}} , \tag{28}$$

and

$$\bar{Y}_2 = \sum_{n=1}^{8} \phi_n A_n e^{\lambda_n \bar{x}} \tag{29}$$

Equations (28) and (29) now have only eight constants to be determined by applying the boundary and continuity conditions.

Analysis of Parts 2 and 3 of Beam System

The differential equations of motion for the transverse vibration of the beam portions of the system as shown in Figure 2 are:

$$D_j \frac{\partial^4 y_{bj}}{\partial x_j^4} + \rho_j A_j \frac{\partial^2 y_{bj}}{\partial t^2} = 0 . \qquad j = 1, 2. \tag{30}$$

For the special case of identical beams,

$$D_1 = D_2 = E^* I, \text{ and } \rho_1 A_1 = \rho_2 A_2 = \rho A.$$

Assuming $y_{bj} = Y_{bj}(x)\, e^{i\omega t}$, j = 1, 2, Equation (30) becomes

$$\frac{d^4 Y_{bj}}{dx_j^4} - \left[\frac{\rho A}{E^* I}\right] \omega^2 Y_{bj} = 0, \; j = 1, 2 . \tag{31}$$

In non-dimensional form,

$$\frac{d^4 \bar{Y}_{bj}}{d\bar{x}_j^4} - \omega^2 \bar{Y}_{bj} = 0, \; j = 1, 2. \tag{32}$$

The solutions of the above equations are obtained, as before by assuming a series solution of the form:

$$\bar{Y}_{b1} = \sum_{i=1}^{4} C_n e^{\beta_n \bar{x}} , \text{ and } \bar{Y}_{b2} = \sum_{i=1}^{4} D_n e^{\beta_n \bar{x}} . \tag{33}$$

where $\beta_n^4 = \bar{\omega}^2$, and C_n and D_n are constants to be found from the boundary conditions.
Equations (28), (29), and (33) have 16 unknown constants. The following boundary and continuity conditions are applied to determine those constants and to obtain the frequency equation.

II. BOUNDARY CONDITIONS

Considering simply-supported boundaries at the un-jointed ends of the two beams, at points 1 and 2 (see Figure 5), the transverse displacement and slope are zero. i.e.

$$\text{a) at } \bar{x}_1 = 0,\ \bar{Y}_{b1} = 0, \text{ and } \frac{d\bar{Y}_{b1}}{d\bar{x}_1} = 0, \tag{34}$$

and

$$\text{b) at } \bar{x}_2 = \bar{\ell},\ \bar{Y}_{b2} = 0, \text{ and } \frac{d\bar{Y}_{b2}}{d\bar{x}_2} = 0. \tag{35}$$

Next, points 3 and 4 are free ends. Hence, the bending moments there are zero. Furthermore, the shear force at these points can be obtained from Equation (16). Hence, we obtain,

c) at $\bar{x} = 0$ (point 3),

$$\frac{d^2\bar{Y}_2}{d\bar{x}^2} = 0, \text{ and } \frac{d^3\bar{Y}_2}{d\bar{x}^3} = \frac{6\bar{G}_c^*}{\bar{h}^2}\left[\frac{d\bar{Y}_1}{d\bar{x}} + \frac{d\bar{Y}_2}{d\bar{x}}\right], \tag{36}$$

d) at $\bar{x} = \bar{\ell}_c$ (point 4),

$$\frac{d^2\bar{Y}_1}{d\bar{x}^2} = 0, \text{ and } \frac{d^3\bar{Y}_1}{d\bar{x}^3} = \frac{6\bar{G}_c^*}{\bar{h}^2}\left[\frac{d\bar{Y}_1}{d\bar{x}} + \frac{d\bar{Y}_2}{d\bar{x}}\right]. \tag{37}$$

Referring to Figure 5, at points A and B, we equate the displacements, slopes, bending moments, and shear forces for the two hypothetical sections of the beams. These will yield eight more equations. Hence we have a matrix equation from the above 16 conditions containing 16 constants. The determinant of the above matrix D, set equal to zero gives the frequency equation, i.e., for a non-trivial solution

$$\text{Det } [D]_{16\times16} = 0. \tag{38}$$

The roots of Equation (38) yield the complex natural frequencies (ω_ns) of the system.

$$\bar{\omega}_{nj} = \bar{\omega}_{Rj} + i\,\bar{\omega}_{Ij},$$

where j = 1, 2, ... represents the mode number.

ω_{Rj} = modal damped natural frequency, and

$\eta_j = \dfrac{\omega_{Ij}}{\omega_{Rj}}$ = modal loss factor.

Once the eigenvalues are evaluated, the corresponding eigenvectors needed to plot the mode shapes can be found by using any 15 of the 16 equations with one arbitrary constant.

III. NUMERICAL RESULTS AND DISCUSSION

The length and thickness of the graphite epoxy beams chosen here for study are: ℓ = 12.25 cm, and h = 0.25 cm. The storage modulus of the beam material as supplied by the manufacturer is 124 GPa. The material loss factor of the beam is taken as η_1 = 0.004, which is taken as a constant for all the modes. This corresponds to a damping ratio of 0.2% and is believed to represent closely the material damping of the graphite epoxy material as found from various previous experiments [13, 14]. The thickness of the adhesive layer is taken as 0.05 cm. The complex modulus of the adhesive material, which is epoxy resin in the present case is taken as 4(1 + i0.04) GPa which has a real part of 4 GPa as supplied by the manufacturer. The complex shear modulus of the adhesive is assumed to be 1.4(1 + i0.04) GPa. Here $\eta_2 = \eta_3 =$ 0.04, which corresponds to a constant damping ratio of 2% for the epoxy material.

The above quantities expressed in non-dimensional form are used in the numerical computation of the eigenvalues and eigenvectors. The ratio of the length of overlap to the beam length is called the overlap ratio. Numerical results are obtained for overlap ratios of 0.2, 0.4, 0.6, and 0.8. Figure 6 shows the variation of natural frequency with overlap ratio for the first three modes of vibration. From this plot, it is clear that the natural frequency of the system increases with an increase in the overlap ratio for all modes. Figure 7 is a similar plot showing the variation of the system damping (total loss factor of the system) with overlap ratio. For the case of overlap ratio = 0.2, the non-dimensional frequencies $\bar{\omega}$ are: 2.86, 13.12 and 27.24 for the first three modes. The corresponding system damping ratios are ζ_1, = 0.534%, ζ_2 = 0.120%, and ζ_3 = 0.054%. It should be noted that the above values were obtained by assuming constant values of ζ = 0.02% and ζ = 2.0% for the material damping ratio of the beam and the adhesive respectively. It is seen that, for this case, the system damping is higher than the material damping of the beam only for the first mode. For the other two modes, the system damping ratio appears to be lower than the material damping ratio of the beam. This observation, however, is true only for the above case and cannot be generalized. To substantiate this point, let us consider a different case in which the damping ratio of the adhesive was assumed to be 5%, and the material damping of the beam was kept the same. The system damping ratios computed for this case are: ζ_1 = 1.66%, ζ_2 = 0.33%, ζ_3 = 0.16%. There were no significant changes in the natural frequencies of the system. As can be seen, the system damping ratios in this case are completely different from the previous case considered. Hence, in order to predict the system damping ratios, using the present model, accurate knowledge about the material damping ratios (of the beam and adhesive) and their dependence on natural frequency is mandatory. Figures 8 shows the predicted mode shapes of the first mode for different overlap ratios.

IV. COMPARISON WITH EXPERIMENTAL RESULTS.

Table 1 shows both theoretical and experimental results of two graphite epoxy lap joint systems with overlap ratios of 0.2 and 0.4. All of the theoretical results were generated by considering simply-supported boundary conditions at the edges.

The specimens were prepared by bonding two similar graphite epoxy beams over the desired length of overlap using an epoxy adhesive. The epoxy resin was procured from CIBA-GEIGY Corporation. Much care was taken to obtain a good bond by properly curing the joint system in an oven. The dimensions of

the unbonded beams are: length = 12.25 cm, width = 2.8 cm, and thickness = 0.25 cm. These dimensions and the material constants (Young's Modulus and Shear Modulus) were input to the computer program to predict the theoretical natural frequencies, modal damping ratios and mode shapes.

The supports to simulate simple-supported boundaries at the ends were specially fabricated in the form of two separate triangular blocks with a knife edge on each, to support the beam, one from top, and the other from bottom. The two blocks were then clamped to a rigid base. In order to evaluate the experimental simulation of these supports, a trail test was first conducted on an aluminum beam. Excellent agreement was obtained between theoretical natural frequencies (computed using simply-supported boundary conditions) and measured values. In fact, the percentage difference between the two results never exceeded 2% for the first four natural frequencies. Having established the validity of the above test fixtures, experiments were later conducted on graphite epoxy lap-jointed beams. An impact hammer with an attached force transducer was used to excite the specimen and the response was measured by a mini-accelerometer (Bruel & Kjaer 4375). The frequency response (ratio of acceleration to force signals) was immediately computed and recorded on a FFT analyzer (Bruel & Kjaer 2032). The modal parameters were then computed using the Structural Measurement Systems (SMS) modal analysis software.

Referring to Table 1 it is seen that there is good agreement between the predicted values of natural frequencies and experimental data. The percentage difference between the two results is in the range of 3 to 9%. The small discrepancies in the two results can be attributed to several assumptions made in the theoretical analysis. The major assumption is the use of a constant value, with frequency of vibration, for the modulus of the material. The measured damping ratio values in column 7 (Table 1) are higher than the predicted values. This is presumably due to additional damping contributions at the end supports in the experimental data. In order to substantiate this, damping measurements were made on the same samples without the end fixtures. Column 8 of Table 1 shows these results. In this case, testing was done by simply mounting the sample directly on a shaker using a thin layer of wax. The resonance frequencies in this case were, of course, somewhat different from those obtained previously using the simply-supported boundary conditions. But, it is interesting to notice that the predicted damping values in column 6 and the measured data in column 8 are of the same order. Next, theoretical mode shape is compared with experimental mode shape in Figure 9 for mode 1. There is excellent agreement between the two mode shapes for the first mode as seen in Figure 9.

V. EXPERIMENTAL STUDY OF DAMPING OF BONDED DOUBLE-BUTT JOINT SPECIMENS

This section contains the results of experiments conducted on beam and double-butt-joint specimens in a vacuum chamber. Damping measurements were made on the following ten graphite epoxy samples which were procured from Sikorski Aircraft Company:

i) Five identical graphite epoxy beam specimens with a double-butt joint in the middle as shown in Figure 10 and ii) Five identical graphite epoxy beam specimens of dimensions as in I but with no joints.

In each of the above experiments, the specimen was mounted at its center directly on the shaker using a thin layer of wax. This closely simulated free-free boundary conditions at the edges. Only odd numbered modes were excited, since the specimen was mounted at the center, which happens to be a node point for all even numbered modes for free-free boundary conditions. All the damping measurements wee made using the usual improved half-power points method as described in [13, 14].

Much care was taken to maintain identical environmental conditions in all of the above experiments. The damping measurements were made precisely by zooming in on each mode thus increasing the frequency resolution of the analyzer and minimizing the influnce of external noise.

First, measurements were made on the double-butt-jointed (DBJ) specimens. In each case, the specimen with the shaker was kept inside the vacuum chamber and damping ratios and resonance frequencies were measured for the first and third mode of vibration, before the air was pumped out. Then the measurements were repeated in a vacuum when the pressure inside the chamber was about 0.1 mm of hg. The test temperature remained ambient in both cases. Table 2 shows a summary of results for the five DBJ specimens tested under vacuum conditions. No significant change in the values of the damping ratio was noticed between the experiments conducted under normal atmospheric pressure and in a vacuum. This difference in the values of the damping ratio was in fact in the range of 0.01-0.02% during most of the trials.

From Table 2, it is seen that the average value of the damping ratio of the DBJ specimen for the first mode is 0.114% and that for the third mode is 0.155%. The small discrepancies in the values of the resonance frequencies in the five samples could be attributed to a) slight differences in their dimension and/or b) slight differences in the exact location of the excitation point during mounting.

The next set of experiments was conducted on the five beam specimens with no joints (having the same dimensions as the DBJ samples) under identical environmental conditions as maintained with the DBJ specimens. The results are tabulated in Table 3. Here, it is seen that the beam has an average value of the damping ratio of 0.107% for the first mode and 0.138% for the third mode.

By comparing the results of Table 2 and 3, it is clear that, although the damping ratio values for the jointed specimens appear somewhat higher than those of the beam specimens, this difference is almost unnoticeable. This observation is also true from the previous damping results of lap-jointed specimens with free-free boundary conditions.

VI. CONCLUSIONS

The analytical model described in this paper can be used to predict the natural frequencies and the modes shapes of a bonded lap joint system for free vibration. The model can also be used to predict the system modal damping values by properly choosing the material damping values of the beam and the adhesive. Good agreement between numerical and experimental results for the natural frequencies of the lap-jointed beam system was obtained. From the numerical and experimental results obtained on lap-jointed beams, it is clear that the natural frequencies of the system increase with an increase in the length of overlap. From the experimental results of bonded lap-joint and bonded butt-joint specimens, the increase in the value of the damping ratio due to the presence of bonded joints in the system does not appear to be very significant. More work is, however, needed in this area to determine if the bonded joints can be relied upon to increase the system damping capacity.

ACKNOWLEDGEMENT

The research work described in this article was conducted at the Sound & Vibration Laboratory of the Mechanical Engineering Department at Auburn University. The research was supported by NASA-MSFC, Huntsville, AL under research contract NAS8-36146. Financial support by NASA is gratefully acknowledged.

REFERENCES

1. Goland, M., and Reissner, E., "The Stresses in Cemented Joints", *Journal of Applied Mechanics*, Vol. 11, March 1944, pp. A17-A27.

2. Ojalvo, I.U., and Eidinoff, H.L., "Bond Thickness Effects upon Stresses in Single-Lap Adhesive Joints", *AIAA Journal*, Vol. 16, No. 3, 1978, pp. 204-211.

3. Carpenter, W.C., "A Comment on Two Current Adhesive Lap Joint Theories", *AIAA Journal*, Vol. 18, No. 3, 1980, 350-352.

4. Kline, R.A., "Stress Analysis of Adhesively Bonded Joints," *Adhesive Joints*, ed. by Mittal, K.L., proc. of the International Symp. on Adhesive Joints, Sept. 1982, Kansas City, Missouri, pp. 587-609.

5. Delale, F., and Erdogan, F., "Viscoelastic Analysis of Adhesively Bonded Joints, "*Journal of Applied Mechanics*, Vol. 48, June 1981, pp. 331-336.

6. Renton, W.J., and Vinson, J.R., "Analysis of Adhesively Bonded Joints Between Panels of Composite Materials," *Journal of Applied Mechanics*, March 1977, pp. 101-106.

7. Delale, F., Erdogan, F., and Aydinoglu, M.N., "Stresses in Adhesively Bonded Joints - A closed form solution," *J. Composite Materials*, Vol. 15, May 1981, pp. 249-271.

8. Hart-Smith, L.J., "Analysis and Design of Advanced Composite Bonded Joints," *NASA CR-2218*, April 1974.

9. Hart-Smith, L.J., "Adhesive-Bonded Double-Lap Joints", *NASA CR-112235*, January 1973.

10. Hart-Smith, L.J., "Adhesive-Bonded Single Lap Joints", *NASA CR-112236*, January 1973.

11. Hart-Smith, L.J., "Adhesive-Bonded Scarf and Stepped-Lap Joints", *NASA CR-112237*, January 1973.

12. Morgan, M.R., and Sinha, S.C., "Influence of a Viscoelastic Foundation on the Stability of Beck's column: An Exact Analysis", *Journal Sound and Vibration*, 91(1), 1983, pp. 85-101.

13. Rao, M.D., Crocker, M.J., Zhu, G.H. and Raju, P.K., "A Study of the Damping Capacity of Graphite Epoxy Composites in a Vacuum," Proc. of *Inter-Noise 86*, M.I.T., Cambridge, July 1986, pp. 687-692.

14. Rao, M.D., Crocker, M.J. and Guest, S.H., "Experimental Study of Damping of Graphite Epoxy Composite Material of the Space Telescope Truss System," paper presented at the 1987 Design Technology Conferences, Boston, ASME publication DE-Vol 5. (ASME, New York; 1987), pp. 271-277.

SYSTEM – TWO PARALLEL BEAMS WITH A LAP JOINT

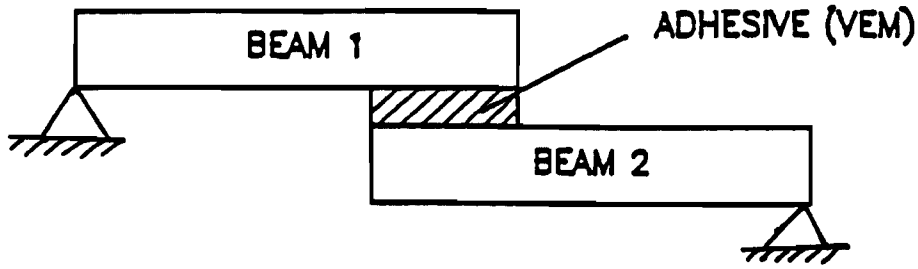

Figure 1. **Two Parallel Beams with a Lap Joint**

ANALYSIS

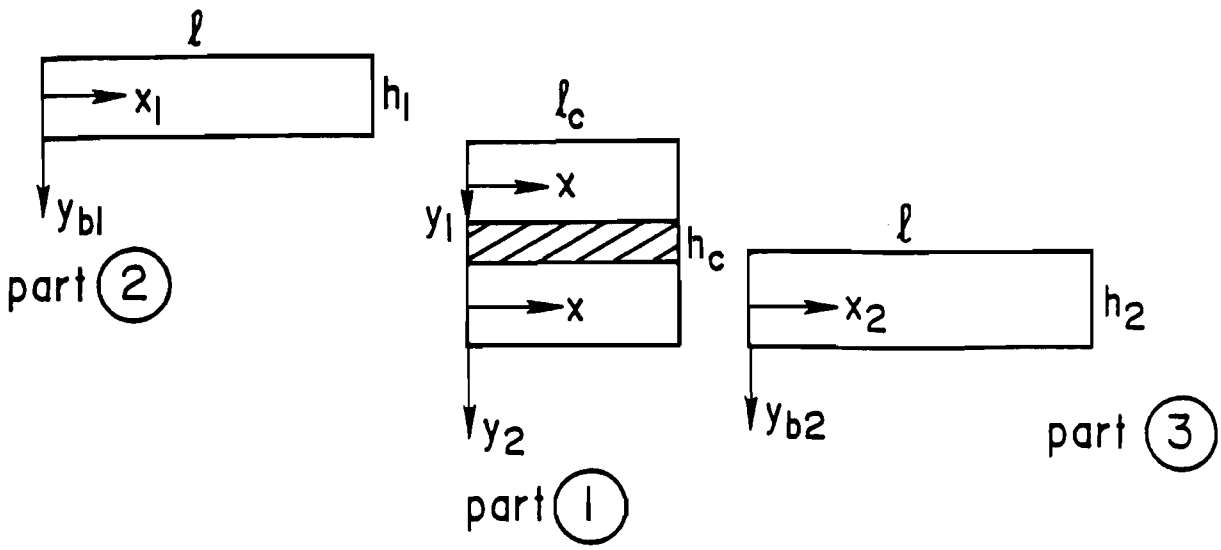

Figure 2. **Hypothetical Division of the System Showing the Coordinates for Analysis**

part 1. FBD

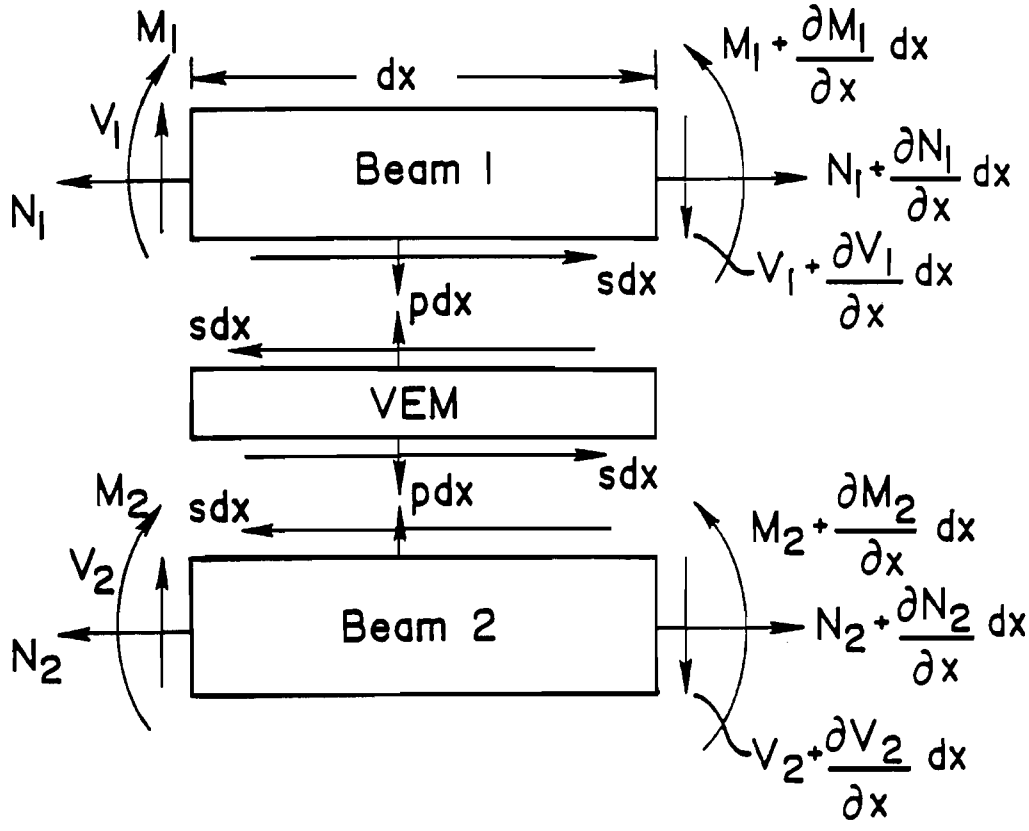

Figure 3. **Free Body Diagram of a Differential Element in the Overlap Region**

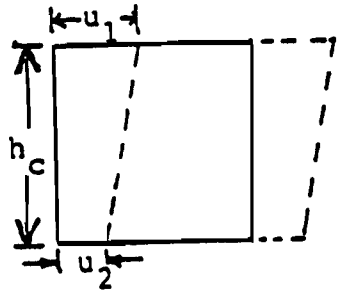

Figure 4. A Small Element of the Viscoelastic Layer

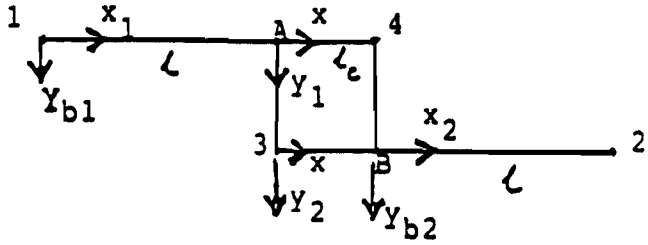

Figure 5. Illustration of the Locations of Boundary and Continuity Conditions

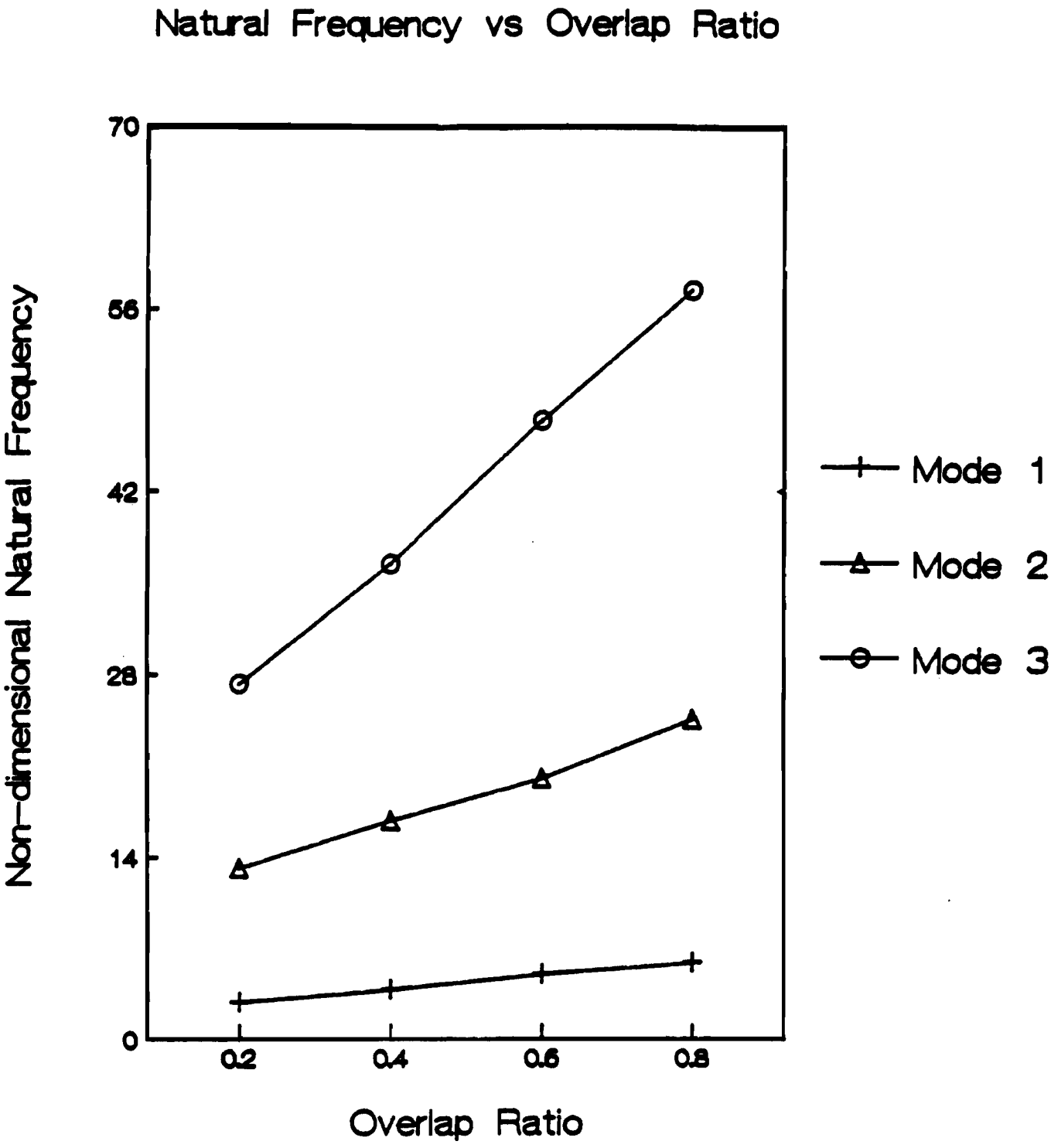

Figure 6. Plot of Natural Frequency vs. Overlap Ratio

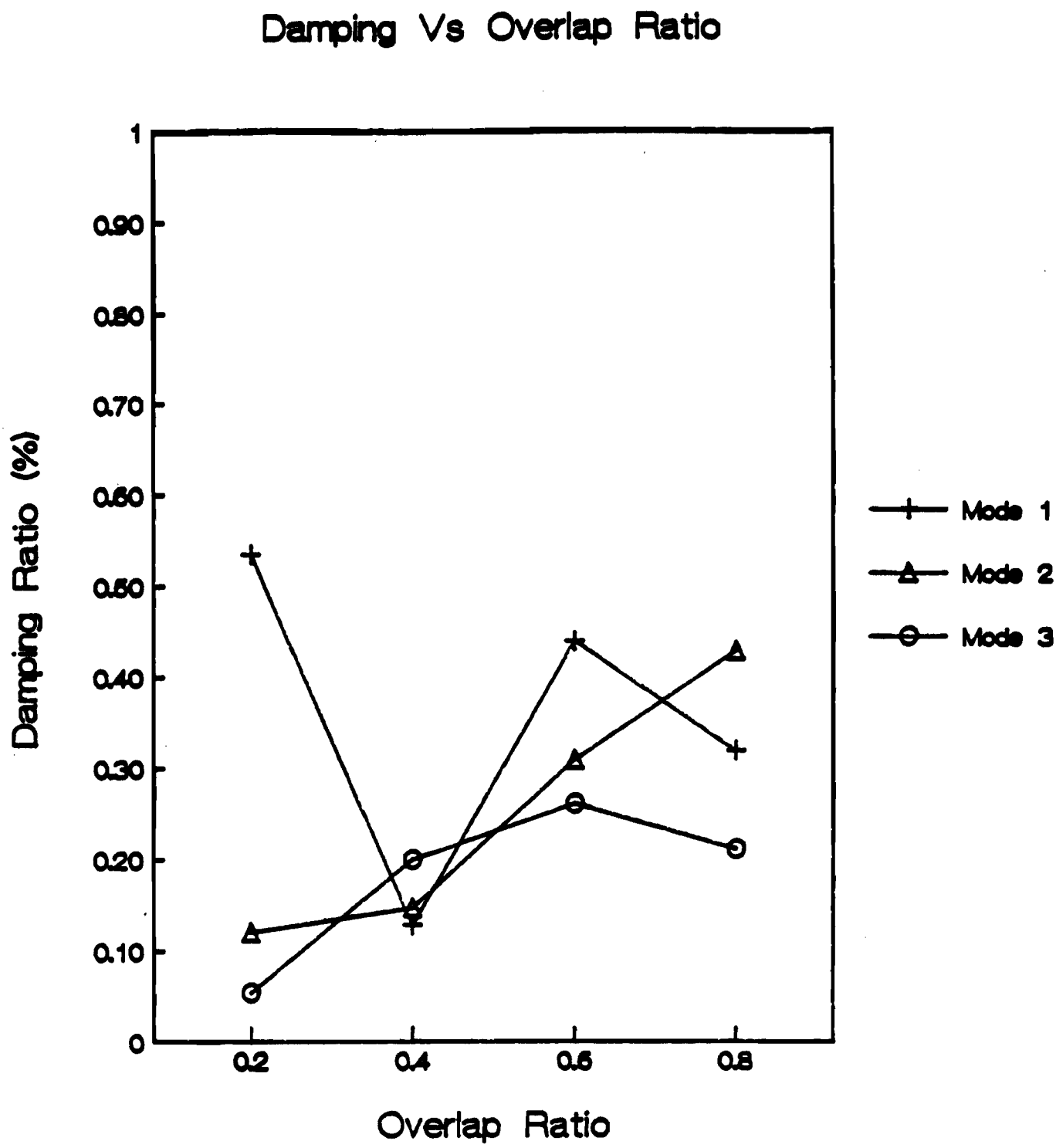

Figure 7. Plot of Damping Ratio vs. Overlap Ratio

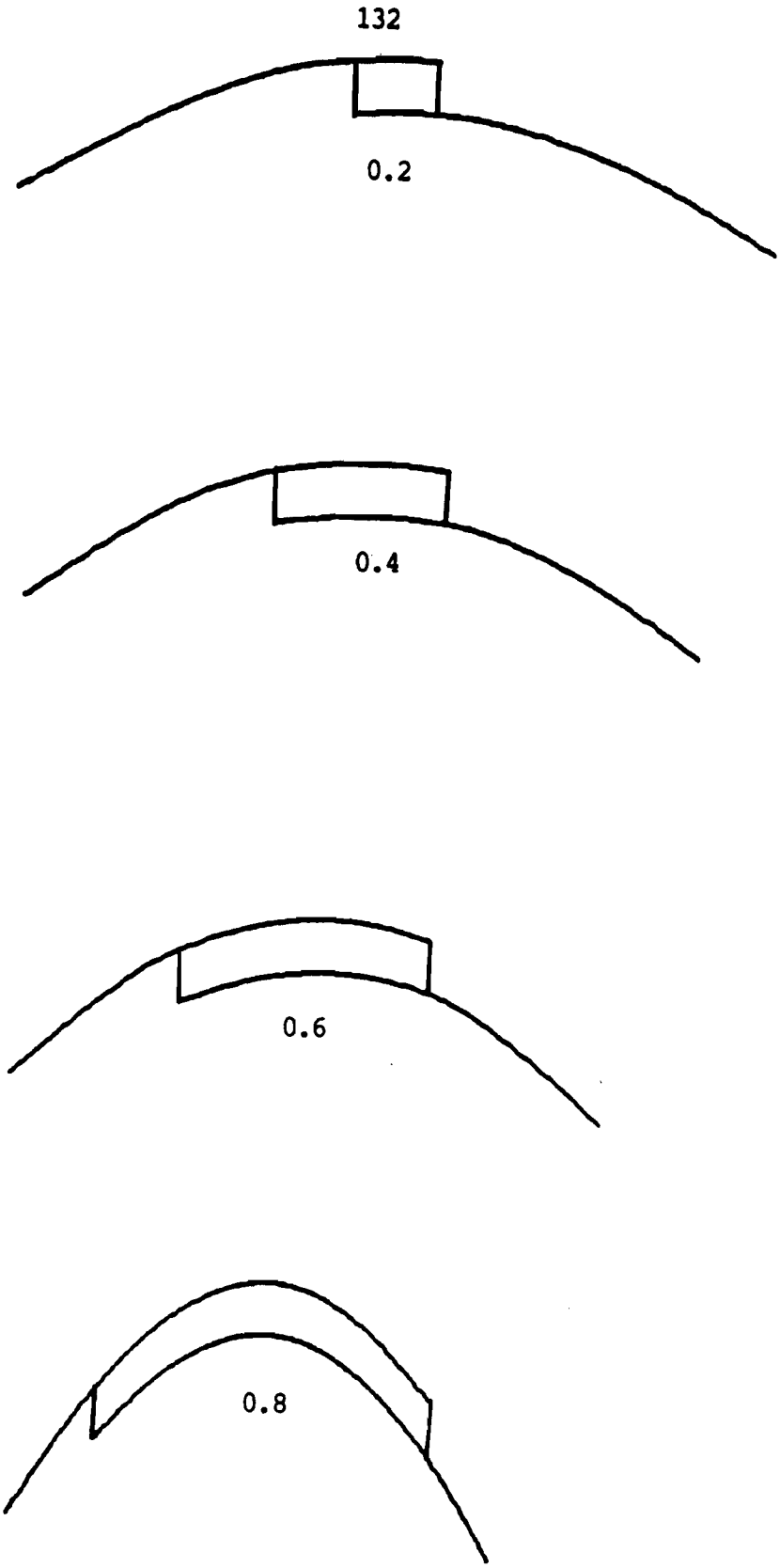

Figure 8. Theoretical Mode Shapes for Mode 1

Overlap Ratio	Mode No.	Natural Frequency(Hz)			Damping Ratio(%)		
		Theory[1]	Expt.[1]	%Error	Theory[1]	Expt.[1]	Expt.[2]
0.2	1	195.90	207.07	5	0.534	1.51	0.20
	2	898.46	986.22	9	0.120	1.63	0.16
	3	1864.49	1984.00	6	0.054	2.29	0.10
0.4	1	263.46	270.60	3	0.128	0.68	0.43
	2	1148.41	1075.49	-6	0.147	1.43	0.12
	3	2492.74	2684.37	7	0.200	0.83	0.15

[1]Using Simply-Supported boundary conditions

[2]Using Free Free boundary conditions.

Table 1. Comparison of Theoretical and Experimental Results of the Graphite Epoxy Lap Joint Systems

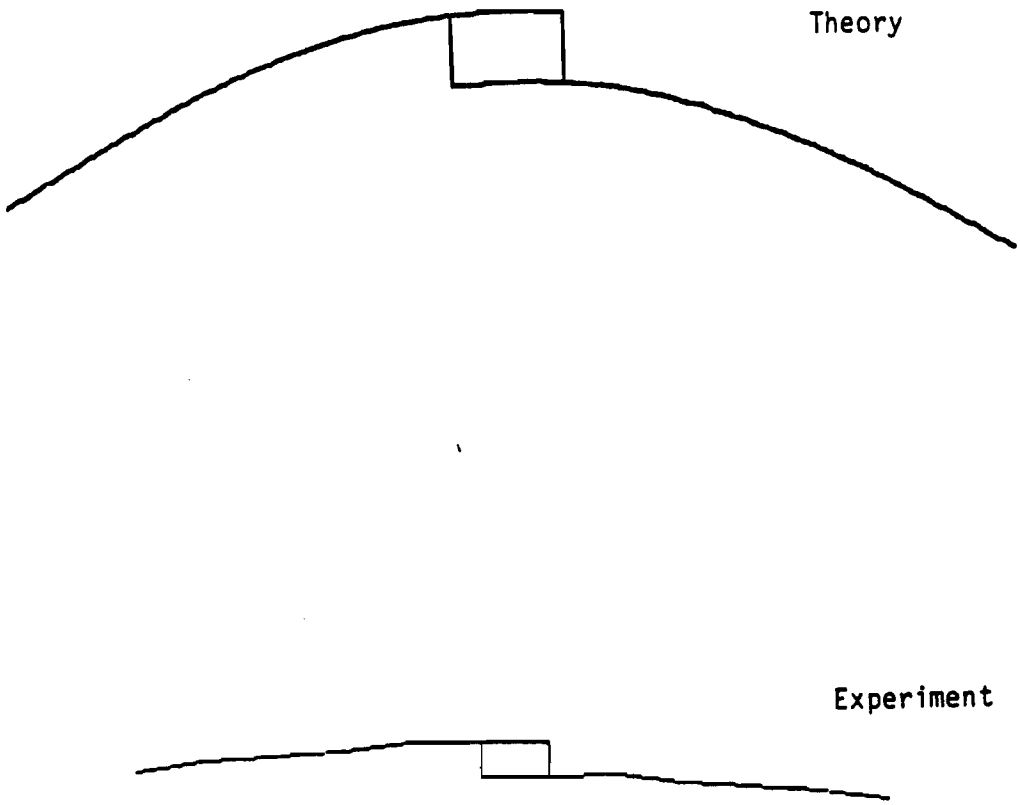

Figure 9. **Comparison of Theoretical and Experimental Mode Shapes for Overlap Ratio = 0.2, Mode 1**

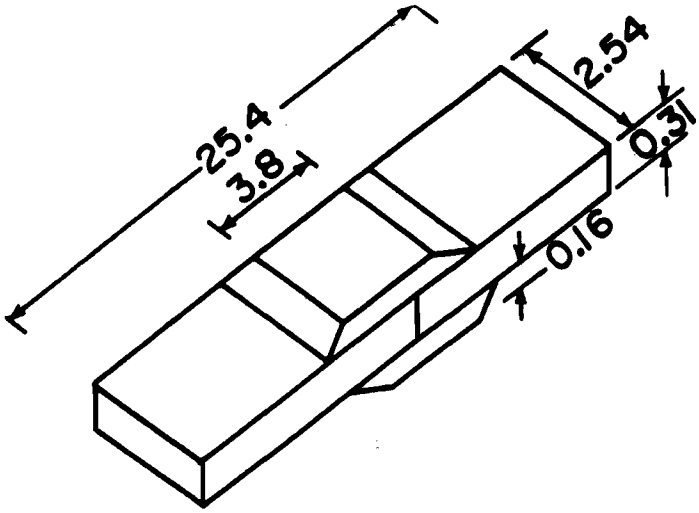

Double-Butt-Jointed Specimen

Table 2.

Sample No.	Damping Ratio	
	Mode 1 (259 Hz)	Mode 3 (1376 Hz)
1	0.113%	0.144%
2	0.102%	0.126%
3	0.127%	0.169%
4	0.105%	0.174%
5	0.122%	0.162%
Average	0.114%	0.155%

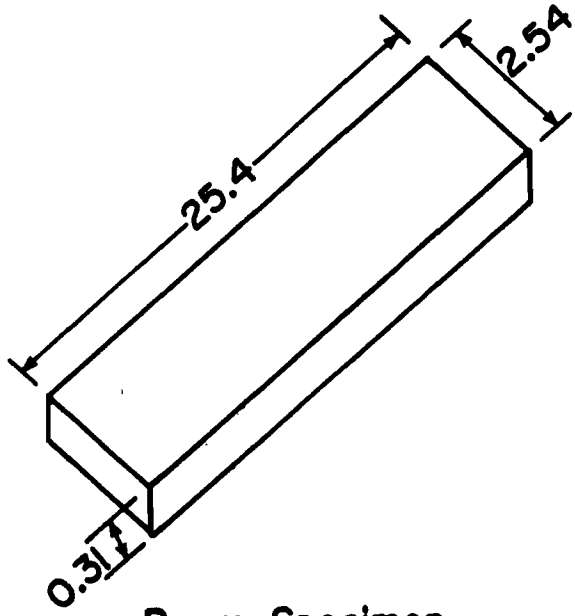

Beam Specimen

All dimensions in cm.

Table 3.

Sample No.	Damping Ratio	
	Mode 1 (337 Hz)	Mode 3 (1779 Hz)
1	0.108%	0.148%
2	0.126%	0.149%
3	0.106%	0.123%
4	0.108%	0.122%
5	0.091%	0.149%
Average	0.107%	0.138%

Figure 10. Experimental Results of Double-Butt Jointed and Beam Specimens